COMMISSION A:
Electromagnetic Metrology, Electromagnetic measurements and standards
(November 2016 – October 2020)

Edited by

Hidekazu Hachisu (National Institute of Information and Communications Technology; NICT) and

Masami Yasuda (National Institute of Advanced Industrial Science and Technology, National Metrology Institute of Japan; AIST, NMIJ)

A1. Time and Frequency Standards and Time Transfer Technique

The research and development on time and frequency standards as well as, time and frequency transfer in Japan are mainly carried out at the National Metrology Institute of Japan (NMIJ) and the National Institute of Information and Communications Technology (NICT).

At NMIJ, the second cesium fountain, NMIJ-F2, for primary frequency standards has been developed. We evaluated the frequency shifts due to the microwave leakage and distributed cavity phase. By measuring the frequency of NMIJ-F2 as a function of the microwave pulse area, the frequency correction and uncertainty for the microwave leakage shift were evaluated to be $(-1.1 \pm 2.5) \times 10^{-16}$. Furthermore, by measuring the frequency of NMIJ-F2 with changes of the tilt angle of the fountain, the frequency correction and uncertainty for the distributed cavity phase shift were evaluated to be $(0 \pm 3.4) \times 10^{-16}$. By these, the uncertainty evaluation of NMIJ-F2 was completed. The type A uncertainty for measurement for 20 d and the type B uncertainty are typically 1.9×10^{-16} and 5.5×10^{-16}, respectively. Ultrastable microwave oscillators: The 3rd cryo-refrigerator-cooled cryogenic sapphire-resonator oscillator (cryoCSO) has been set up. The Allan deviations of 3 cryo-CSOs were evaluated by the three-cornered-hat method, to be 2×10^{-15}, 3×10^{-15}, and 4×10^{-15} at an averaging time of 1 s, respectively. One of the cryoCSOs has been continuously operating, except during an annual scheduled power outage due to an inspection of electrical facilities. At present three active hydrogen maser frequency standards and one cesium atomic clock with high-performance beam tubes (Agilent 5071A) are operated at NMIJ for time keeping. Those atomic clocks are kept in individual chambers, whose temperature variations are kept to within 0.2 deg C. One of the hydrogen masers is used as a source oscillator for generating UTC (NMIJ), which is created by frequency-steering of the hydrogen maser output signal using a frequency stepper (AOG). At NMIJ, Dual frequency carrier phase GPS receiver is one of the main international time and frequency transfer tools. NMIJ has the Two Way Satellite Time and Frequency Transfer (TWSTFT) facilities for Asia Pacific link and for Asia-European link.

Frequency Calibration Service at NMIJ; NMIJ has been providing the remote frequency calibration service using the GPS common-view method and Internet since 2006. The CMCs of the service are 1.1×10^{-13} (baseline: 50 km), 1.4×10^{-13} (baseline: 500 km) and 4.9×10^{-13} (baseline: 1,600 km) at an averaging time of one day. The number of users is 19 in 2021.

NICT maintains Japan Standard Time (JST) and disseminates it domestically. From 2016 to 2020, the time difference of UTC(NICT) from UTC was kept within approximately 20 ns. In 2018, a substation in Kobe was opened with the purpose of distributed and integrated management of JST. Currently, it continually operates as an emergency backup station for the Tokyo headquarters. NICT established a new precise frequency transfer method for two-way satellite time and frequency transfer (TWSTFT), named two-way satellite carrier-phase frequency transfer (TWCP) and developed a frequency measurement system of optical clocks without a flywheel oscillator [Fujieda *et al*., 2016]. Additionally, NICT and KRISS succeeded in the optical clock comparison of Sr and Yb optical lattice clocks by TWCP, where an uncertainty at the mid-10^{-16} level was achieved after a total measurement time of 12 hours [Fujieda *et al*., 2018]. NICT subsequently developed a new digital TWSTFT modem to enable TWCP and time transfer by code phase [Fujieda *et al*., 2020]. The performance of the new modems has been evaluated in Japanese and Asian TWSTFT links in collaboration with KRISS and TL since 2019. In National Metrology Institutes (NMIs), the implementation of software defined receiver (SDR) has actively proceeded into the TWSTFT earth stations to reduce instabilities with daily variation [Jiang *et al*., 2018]. By adapting TWCP to wireless communication modules, wireless two-way interferometry (Wi-Wi), was developed at NICT [Shiga *et al*., 2017]. Wi-Wi has already been applied to monitor distance variations [Bohla *et al*., 2019] and water vapor in the atmosphere [Yasuda *et al*., 2019] at a mm level of accuracy. The development of a microfabricated atomic clock has been started in NICT. By using piezoelectric MEMS (Micro Electro-Mechanical System) and CMOS technologies, an ultra-compact RF oscillator for a Rb atomic clock was developed. Its operation was verified by incorporating it into a CPT atomic clock system [Hara *et al*., 2018]. Furthermore, to compress the physics package height, a reflection-type gas cell was developed by integrating an optical MEMS device into the gas cavity [Nishino *et al*., 2019]. An atomic clock test bench and a fast CPT simulator were also developed to accelerate the development activity [Yano *et al*., 2017] [Yano *et al*., 2019]. By using a custom-designed broadband feed [Ujihara *et al*., 2018], NICT developed a broadband VLBI (Very Long Baseline Interferometry) system for long-distance precise frequency transfer. Transportable 2.4 m diameter VLBI terminals were installed at NICT (Japan) and INAF (National Institute for Astrophysics, Italy) for frequency ratio measurement between the Sr optical lattice clock at NICT and an Yb optical lattice clock at INRIM (National Institute of Metrological Research, Italy). VLBI observations were conducted pairing these two small antennas with the Kashima 34 m radio telescope in 2018-2019 [Pizzocaro *et al*., 2021] [Sekido *et al*., 2021]. The

Kashima 34 m radio telescope used in this project was forced to end its operation due to serious damage caused by the typhoon Faxai on 9 Sep. 2019 and it was dismantled in 2020. This telescope had been constructed as an element of the Western Pacific Radio Interferometer in 1988 and played an important role in VLBI technology developments and international observations in the field of geodesy and astronomy.

[References]

Bhola R P, Kido K, Yasuda S, Hanado Y, Kawamura S, Hanado H, Takizawa K, Inoue M, and Shiga N [2019], “Distance Variation Monitoring with Wireless Two-way Interferometry (Wi-Wi),” Sens. Mater. **31** (7), 2313-2321.

Fujieda M, Ido T, Hachisu H, Gotoh T, Takiguchi H, Hayasaka K, Toyoda K, Yonegaki K, Tanaka U, and Urabe S [2016], “Frequency measurement system of optical clocks without a flywheel oscillator,” IEEE Trans. Ultrason. Ferroelectr. Freq. Control. **63** (12), 2231-2236

Fujieda M, Yang S-H, Gotoh T, Hwang S-W, Hachisu H, Kim H, Lee Y-K, Tabuchi R, Ido T, Lee W-K, Heo M-S, Park C-Y, Yu D-H, Petit G [2018], “Advanced Satellite-based Frequency Transfer at the 10^{-16} Level,” IEEE Ultrason. Ferroelectr. Freq. Control **65** (6), 973-978.

Fujieda M, R. Tabuchi, T. Gotoh [2020], “DEVELOPMENT OF A NEW DIGITAL TWSTFT MODEM”, Int. J. Electr. Eng. **27** (4), 141-145.

Hara M, Yano Y, Kajita M, Nishino H, Ibata Y, Toda M, Hara S, Kasamatsu A, Ito H, Ono T, and Ido T [2018], “Microwave oscillator using piezoelectric thin-film resonator aiming for ultraminiaturization of atomic clock,” Rev. Sci. Instrum. **89** (10), 105002.

Jiang Z, Zhang V, Huang Y-J, Achkar J, Piester D, Lin S-Y, Wu W, Naumov A, Yang S-H, Nawrocki J, Sesia I, Schlunegger C, Yang Z, Fujieda M, Czubla A, Esteban H, Rieck C, Whibberley P [2018], “Use of software-defined radio receivers in two-way satellite time and frequency transfers for UTC computation,” Metrologia **55**, 685-698.

Nishino H, Yano Y, Hara M, Toda M, Kajita M, Ido T, and Ono T [2019], “Reflection-type vapor cell for micro atomic clocks using local anodic bonding of 45° mirrors,” Opt. Lett. **46** (10), 2272-2275.

Pizzocaro M, Sekido M, *et al*. [2021] “Intercontinental comparison of optical atomic clocks through very long baseline interferometry," Nat. Phys. **17**(2), 223-227, DOI: 10.1038/s41567-020-01038-6.

Sekido M, *et al*., [2021] "A broadband VLBI system using transportable stations for geodesy and metrology - An alternative approach to the VGOS concept -," J Geod **95** (41), DOI: 10.1007/s00190-021-01479-8 25.

Shiga N., Kido K, Yasuda S, Patna B, Hanado Y, Kawamura S, Hanado H, Takizawa K, and Inoue M [2017], "Demonstration of wireless two-way interferometry (Wi-Wi)," IEICE Communications Express **6** (2), 77-82.

Ujihara H, *et al*. [2019], "Development of wideband antennas", International Symposium on Advancing Geodesy in a Changing World, DOI: 10.1007/1345_2018_41.

Yano Y, Goka S and Kajita M [2017], "Two-step pulse observation to improve resonance contrast for coherent population trapping atomic clocks," Appl. Phys. B **123**, 67 1-8

Yano Y, Kajita M, Ido T, and Hara M [2019], "Fast numerical analysis of the time response in coherent population trapping resonance based on Galerkin spectral method," Jpn. J. Appl. Phys **58** (SG), SGGB05.

Yasuda S, Ichikawa R, Hanado Y, Kawamura S, Hanado H, Iwai H, Namba K, Okamoto Y, Fukunaga K, Iguchi T, Shiga N [2019], "Horizontal atmospheric delay measurement using wireless two-way interferometry (Wi-Wi)," Radio Sci. **54**, 572.

A2. Laser Stabilization & Frequency Measurement

The research and development on laser stabilization and frequency measurement at several institutes in Japan.

NICT reported the absolute frequency of an ^{87}Sr optical lattice clock by reference to International Atomic Time (TAI) at an uncertainty of less than 10^{-15} [Hachisu *et al*., 2017a], and reached an uncertainty at the low 10^{-16} level after this [Hachisu *et at*., 2017b]. This contributed to the 2017 update of the CIPM recommendation value. NICT was first to use an optical clock to generate an actual time scale signal for nearly half a year. The measurements over that interval were also used to evaluate the TAI scale interval [Hachisu *et al*., 2018]. The clock was consequentially recognized as a secondary frequency standard in 2018, and has formally participated in TAI calibration after this. The clock measurements also contributed to an international dark matter search led by the Nicolaus Copernicus University in Poland [Wcisło *et al*., 2018]. At NICT, a new frequency standard based on the In^+ $^1S_0$-$^3P_0$ transition frequency is now in development [Ohtsubo *et al*., 2019]. In 2017, a new measurement of the clock frequency of this standard was reported with an uncertainty of 10^{-15} order, which contributed to the update of the CIPM recommended value [Ohtsubo *et al*., 2017]. In 2020, the frequency ratio of In^+/Sr was measured with an uncertainty of 7.7×10^{-16} [Ohtsubo *et al*., 2020]. In theoretical work at NICT, the attainable uncertainty of the vibrational transition frequencies of O_2^+ molecular ion was estimated to be lower than 10^{-17} [Kajita, 2017]. The possibility to establish the frequency standard in the terahertz region was discussed. The $(J, F) = (0,1/2) – (1,1/2)$ (J: rotational state, F: hyperfine state) transition of QH^+ (Q: even isotope of alkali earth atom or rare gas atom) is free from the electric quadrupole shift. Using these molecular ions, trapped in a linear trap and sympathetically cooled, a measurement uncertainty below 10^{-15} is attainable when the magnetic field is maintained to below 1 mG [Kajita *et al*., 2020a] [Kajita *et al*., 2020b]. NICT also developed an apparatus for the frequency comparison of two THz waves at separate locations [Nagano *et al*., 2017].

At NMIJ, the systematic uncertainty of the ^{171}Yb lattice clock ($^1S_0$-$^3P_0$ transition) has been evaluated to be 3.6×10^{-16} in 2018 [Kobayashi *et al*., 2018]. This robust Yb lattice clock with automatic laser frequency re-lock systems [Kobayashi *et al*., 2019] was successfully used for calibrating TAI with uptime ratio of 80 % for six months [Kobayashi *et al*., 2020]. The frequency ratio of the clock transitions in Sr and Yb was measured by an optical direct frequency link between two independent optical lattice clocks of Sr and Yb in 2021. The fractional uncertainty of the measurement was 4.1×10^{-16} [Hisai *et al*., 2021].

Katori group at the University of Tokyo and RIKEN has developed optical lattice clocks to establish accurate frequency standards, and is exploring applications in fundamental physics and relativistic geodesy. They have investigated higher-order lattice light shifts to reduce the uncertainty of the clock to less than 10^{-18}, and determined the optimal parameters for the frequency and intensity of the lattice laser with Sr [Ushijima *et al*., 2018] and Yb atoms [Nemitz *et al*., 2019]. The frequency ratio between the different clock transitions gives insight into exploring fundamental physics and validation of measurements that support the redefinition of the second. They have demonstrated cooling of Cd atoms as a new candidate for OLCs [Yamaguchi *et al*., 2019], developed stable single-branch Er-combs for frequency comparison [Ohmae *et al*., 2017], compared ^{87}Sr and ^{88}Sr isotopes [Takano *et al*., 2017], and completed the loop closure over the frequency ratios among Sr, Yb, and Hg atoms [Ohmae *et al*., 2020]. They have also developed a transportable optical lattice clock that operates with an uncertainty of 10^{-18} even in the field environment. A pair of clocks was transported to TOKYO Skytree to test general relativity with an uncertainty of 10^{-5}, comparable to that of space experiments [Takamoto *et al*., 2020]. A long-distance optical fiber link was developed between RIKEN, the University of Tokyo, and NTT for application in future optical lattice clock networks [Akatsuka *et al*., 2020]. Other applications of magic-wavelength protocols have also been explored, such as atomic interferometry in magic-wavelength dipole traps [Akatsuka *et al*., 2017], superradiant clocks inside hollow-core fibers [Okaba *et al*., 2019], and mid-infrared laser cooling in metastable states of Sr atoms for continuous operation of OLCs [Hashiguchi *et al*., 2019].

Hong group at Yokohama National University is developing optical frequency combs and frequency stabilized lasers. They have developed a low-repetition-rate dual comb spectrometer for molecular spectroscopy [Ikeda *et al*., 2020]. They have also developed an iodine-stabilized laser at telecom wavelength for applications including optical frequency standards [Ikeda *et al*., 2020]. Prof. Hong has summarized recent research activities of optical frequency standards in a review article [Hong, 2017].

Sugiyama group at Kyoto University has been developing Yb^+ and Ba^+ ion clocks. The group aims at search for a temporal variation of the fine-structure constant and precise measurement of isotope shifts. Micromotion minimization has been improved in three dimensions for a conventional RF trap and a linear RF trap. Optical frequency-ratio measurement systems has been developed using octave-spanning optical frequency combs based on a mode-locked titanium-sapphire laser [Hatanaka *et al*., 2017] and a ytterbium-doped potassium-yttrium-tungstate (Yb:KYW) lasers [Mitaki *et al*., 2018] [Mitaki *et al*., 2021].

Nakagawa group at University of Electro-communications (UEC) has developed an optical frequency synthesizer for the precision spectroscopy of Rydberg states of Rb atoms using an Er fiber-based optical frequency comb. They demonstrate the high resolution spectroscopy of the *nD* (n=53-92) and *nS* (n=60-90) Rydberg states of ^{87}Rb and measure the absolute frequencies of these transitions with an uncertainty of 250 kHz [Watanabe *et al*., 2017]. They have also developed a quantum simulator based on cold Rydberg atoms in microtrap arrays, and demonstrate quantum many-body dynamics of Ising-type quantum spin model with up to six interacting spins [Tamura *et al*., 2020].

Musha group at UEC has developed the space-borne precision microwave frequency reference for Japanese next-generation quasi-zenith satellite, whose frequency stability reaches 10^{-15} level for averaging time of more than 1000 s. The optical frequency reference from the iodine-stabilized fiber DFB laser at 1 um is down-converted to the microwave region without phase noise degradation by using an optical frequency comb. For the space-borne optical frequency comb, the robust fiber mode-lock laser has been developed which consists of all-PM figure-8 type NALM oscillator [Takeuchi *et al*., 2020]. For the compact and robust trapping light source for the Sr optical lattice clock, a Tm-doped ZBLAN fiber MOPA (master oscillator power amplifier) has developed. By utilizing self-breaching effect for compensating photodarkening, a stable operation of 2-W narrow-linewidth 813-nm light has been achieved [Kajikawa *et al*., 2019]. We have also developed a space borne high-power and highly-stabilized laser for the space gravitational wave detector DECIGO [Suemasa *et al*., 2017, 2018]

Goka group at Tokyo Metropolitan University (TMU) is developing chip-scale atomic clocks. They have developed gas-cell based miniature atomic clocks with better frequency stabilities by using improvement methods. A frequency drift detection method was demonstrated using a dual alkali microelectromechanical system (MEMS) cell to improve the long-term stability [Furuse *et al*., 2017]. A two-step pulse observation method in a two-step Raman–Ramsey scheme was proposed and showed a good contrast and lower light-shift of the coherent population trapping (CPT) resonances [Yano *et al*., 2017]. A miniaturized ultralow-power atomic clock (ULPAC) with the frequency stability of 2.2×10^{-12} at an averaging time of 10^5 s and 59.9 mW power consumption was demonstrated [Zhang *et al*., 2019]. The ULPAC was operated with a proposed frequency drift reducing method [Yanagimachi *et al*., 2020].

[References]

Akatsuka T, Takahashi T, and Katori H [2017], "Optically guided atom interferometer tuned to magic wavelength," Appl. Phys. Express **10**, 112501.

Akatsuka T, Goh T, Imai H, Oguri K, Ishizawa A, Ushijima I, Ohmae N, Takamoto M, Katori H, Hashimoto T, Gotoh H, and Sogawa T [2020], "Optical frequency distribution using laser repeater stations with planar lightwave circuits," Opt. Express **28**, 9186.

Furuse Y, Kase Y, Goka S [2017], "Frequency drift detection method using dual alkali gas for coherent population trapping atomic clocks," 2017 Joint Conference of the European Frequency and Time Forum and IEEE International Frequency Control Symposium (EFTF/IFCS), 328-331.

Hachisu H, Petit G, and Ido T [2017a] "Absolute frequency measurement with uncertainty below 1×10^{-15} using International Atomic Time," Appl. Phys. B **123**, 34 1-5.

Hachisu H, Petit G, Nakagawa F, Yuko Y, and Ido T [2017b], "SI-traceable measurement of an optical frequency at the low 10^{-16} level without a local primary standard," Opt. Express **25**, 8511.

Hachisu H, Nakagawa F, Hanado Y, and Ido T [2018], "Months-long real-time generation of a time scale based on an optical clock," Sci. Rep. **8**, 4243.

Hashiguchi K, Akatsuka T, Ohmae N, Takamoto M, and Katori H [2019], "Frequency measurement on the 5s5p $^3P_2$ - 5s4d $^3D_3$ transition of ^{88}Sr atoms using the photon-momentum-transfer technique," Phys. Rev. A **100**, 042513.

Hatanaka S, Sugiyama K, Mitaki M, Misono M, Slyusarev S N, and Kitano M [2017], "Phase locking of a mode-locked titanium-sapphire laser-based optical frequency comb to a reference laser using a fast piezoelectric actuator," Appl. Opt. **56**(12), 3615-3621.

Hisai Y, Akamatsu D, Kobayashi T, Hosaka K, Inaba H, Hong F-L, Yasuda M [2021], "Improved frequency ratio measurement with ^{87}Sr and ^{171}Yb optical lattice clocks at NMIJ," Metrologia **58**, 015008.

Hong F-L [2017], "Optical frequency standards for time and length applications," Meas. Sci. Technol. **28**, 012002.

Ikeda K, Yamada Y, Kato H, Yoshii K, Okubo S, Inaba H, and Hong F-L [2020], "Development of 19.8-MHz-repetition-rate optical frequency combs for dual-comb spectroscopy," Jpn. J. Appl. Phys. **59**, 028002.

Ikeda K, Okubo S, Wada M, Kashiwagi K, Yoshii K, Inaba H, and Hong F-L [2020], "Iodine-stabilized laser at telecom wavelength using dual-pitch periodically poled lithium niobate waveguide," Opt. Express **28**, 2166.

Kajikawa E, Ishii T, Kubo T, Takeuchi Y, Ogawa K, Musha M [2019], "Dual-wavelength-pumped Tm^{3+}-doped ZBLAN fiber MOPA at 813 nm," Opt. Lett. **44**, 2875-2878.

Kajita M [2017], "Accuracy estimation of the $^{16}O_2^+$ transition frequencies targeting the search for the variation in the proton-electron mass ratio," Phys. Rev. A **95**, 023418 1-6.

Kajita M, Bala R, and Abe M [2020a], "Attainable accuracies of QH^+ rotational transition frequencies (Q:^{40}Ca, ^{24}Mg, ^{202}Hg)," J. Phys. B At. Mol. Opt. Phys. **53**, 085401.

Kajita M and Kimura N [2020b], "Prospect in rare-gas hydride ions for terahertz frequency standards," J. Phys. B At. Mol. Opt. Phys. **53**, 135401.

Kobayashi T, Akamatsu D, Hisai Y, Tanabe T, Inaba H, Suzuyama T, Hong F-L, Hosaka K, Yasuda M [2018], "Uncertainty evaluation of an ^{171}Yb optical lattice clock at NMIJ," IEEE Trans. Ultrason. Ferroelectr. Freq. Control, **65**(12), 2449.

Kobayashi T, Akamatsu D, Hosaka K, Yasuda M [2019], "A relocking scheme for optical phase locking using a digital circuit with an electrical delay line," Rev. Sci. Instrum. **90**, 103002.

Kobayashi T, Akamatsu D, Hosaka K, Hisai Y, Wada M, Inaba H, Suzuyama T, Hong F-L, Yasuda M [2020], "Demonstration of the nearly continuous operation of an ^{171}Yb optical lattice clock for half a year," Metrologia **57**, 065021.

Mitaki M, Sugiyama K, and Kitano M [2018], "Octave-spanning optical frequency comb based on a laser-diode pumped Kerr-lens mode-locked Yb:KYW laser for optical frequency measurement," Appl. Opt. **57**(18), 5150-5160.

Mitaki M and Sugiyama K [2021], "Phase-locking of octave-spanning optical frequency comb based on Kerr-lens mode-locked Yb:KYW laser to reference laser," Jpn. J. Appl. Phys. **60**(2), 22003.

Nagano S, Kumagai M, Ito H, Kajita M, and Hanado Y [2017], "Phase-coherent transfer and retrieval of terahertz frequency standard over 20 km optical fiber with 4×10^{-18} accuracy," Appl. Phys. Express **10**, 012502 1-4.

Nemitz N, Jørgensen A, Yanagimoto R, Bregolin F, and Katori H [2019], "Modeling light shifts in optical lattice clocks," Phys. Rev. A **99**, 033424.

Ohmae N, Kuse N, Fermann M E, and Katori H [2017], "All-polarization-maintaining, single-port Er:fiber comb for high-stability comparison of optical lattice clocks," Appl. Phys. Express

10, 062503.

Ohmae N, and Katori H [2019], "626-nm single-frequency semiconductor laser system operated near room temperature for mW-level second-harmonic generation at 313 nm," Rev. Sci. Instrum. **90**, 063201

Ohmae N, Bregolin F, Nemitz N, and Katori H [2020], "Direct measurement of the frequency ratio for Hg and Yb optical lattice clocks and closure of the Hg/Yb/Sr loop," Opt. Express **28**, 15112.

Ohtsubo N, Li Y, Matsubara K, Ido T, and Hayasaka K [2017], "Frequency measurement of the clock transition of an indium ion sympathetically-cooled in a linear trap," Opt. Express **25**, 11725.

Ohtsubo N, Li Y, Nemitz N, Hachisu H, Matsubara K, Ido T, and Hayasaka K [2019], "Optical clock based on a sympathetically-cooled indium ion," Hyperfine Interactions **240**, 39.

Ohtsubo N, Li Y, Nemitz N, Hachisu H, Matsubara K, Ido T, and Hayasaka K [2020], "Frequency ratio of an $^{115}In^{+}$ ion clock and a ^{87}Sr optical lattice clock," Opt. Lett. **45**, 5950.

Okaba S, Yu D, Vincetti L, Benabid F, and Katori H [2019], "Superradiance from lattice-con fined atoms inside hollow core fibre," Commun. Phys. **2**, 136.

Suemasa A, Shimo-oku A, Nakagawa K, Musha M, [2017], "Developments of high frequency and intensity stabilized lasers for space gravitational wave detector DECIGO/B-DECIGO," CEAS space journal **9**, 485-491.

Suemasa A, Shimo-oku A, Ohtsuka S, Nakamori M, Musha M [2018], "Stable and high power 515-nm lasers for the space gravitational wave detector: DECIGO," *Proceedings of ICSO2018* **3c**, 1220.

Takamoto M, Ushijima I, Ohmae N, Yahagi T, Kokado K, Shinkai H, and Katori H [2020], "Test of general relativity by a pair of transportable optical lattice clocks," Nat. Photonics **14**, 411-415.

Takano T, Mizushima R, and Katori H [2017], "Precise determination of the isotope shift of ^{88}Sr – ^{87}Sr optical lattice clock by sharing perturbations," Appl. Phys. Express **10**, 072801.

Takeuchi Y, Saito R, Endo S, Matsusaka K, Musha M [2020], “Development of an all PM mode lock fiber laser for space borne frequency reference,” *Proceeding of SPIE* **11852**, 118523O-2.

Tamura H, Yamakoshi T and Nakagawa K [2020], “Analysis of coherent dynamics of a Rydberg-atom quantum simulator,” Phys. Rev. A **101**, 043421 1-8.

Ushijima I, Takamoto M, Katori H [2018], “Operational Magic Intensity for Sr Optical Lattice Clocks,” Phys. Rev. Lett. **121**, 263202.

Watanabe N, Tamura H, Musha M, and Nakagawa K [2017], “Optical frequency synthesizer for precision spectroscopy of Rydberg states of Rb atoms,” Jpn. J. Appl. Phys. **56**, 112401 1-5.

Wcisło P., P. Ablewski, K. Beloy, S. Bilicki, M. Bober, R. Brown, R. Fasano, R. Ciuryło, H. Hachisu, T. Ido, J. Lodewyck, A. Ludlow, W. McGrew, P. Morzyński, D. Nicolodi, M. Schioppo, M. Sekido, R. Le Targat, P. Wolf, X. Zhang, B. Zjawin, and M. Zawada [2018], “New bounds on dark matter coupling from a global network of optical atomic clocks,” Sci. Adv. **4**, eaau4869.

Yamaguchi A, Safronova M S, Gibble K, and Katori H [2019], “Narrow-line Cooling and Determination of the Magic Wavelength of Cd,” Phys. Rev. Lett. **123**, 113201.

Yanagimachi S, Harasaka K, Suzuki R, Suzuki M, Goka S [2020], “Reducing frequency drift caused by light shift in coherent population trapping-based low-power atomic clocks,” Appl. Phys. Lett. **116**, 104102.

Yanagimoto R, Nemitz N, Bregolin F, and Katori H [2018], “Decomposed description of Ramsey spectra under atomic interactions,” Phys. Rev. A **98**, 012704.

Yano Y, Goka S, Kajita M [2017], “Two-step pulse observation to improve resonance contrast for coherent population trapping atomic clock,” Appl. Phys. B **123**, 67.

Zhang H, Herdian H, Narayanan A T, Shirane A, Suzuki M, Harasaka K, Adachi K, Goka S, Yanagimachi S, Okada K [2019], “ULPAC: A Miniaturized Ultralow-Power Atomic Clock,” in IEEE Journal of Solid-State Circuits **54**(11), 3135-3148.

A3. Realization of Electrical Unit (DC & LF)

Research works and developments on dc and low frequency electrical standards are implemented in the electrical standards area of Research Institute for Physical Measurement in NMIJ, partly in collaboration with several other institutes in the Advanced Industrial Science and Technology (AIST). In the five research groups of the electrical standards area, the Applied Electrical Standards Group and the Quantum Electrical Standards Group covers A3 Field.

A liquid-helium-free PJVS has been utilized since 2015 for calibrations of Zener voltage standards with the CMC values, 8 nV for 1 V and 45 nV for 10 V, same as those for our conventional JVS system cooled with liquid helium. We are now attempting to develop an AC voltage calibration system using PJVS. Development of Zener voltage standards are also now in progress in collaboration with ADC Corporation. We are continuing to investigate the environmental-condition dependences of the voltage outputs of prototype Zener modules (Fig. 3.1). Excelent stability in the nominal 10 V and 7.2 V outputs for temperature, ambient-pressure and relative-humidity changes has been confirmed.

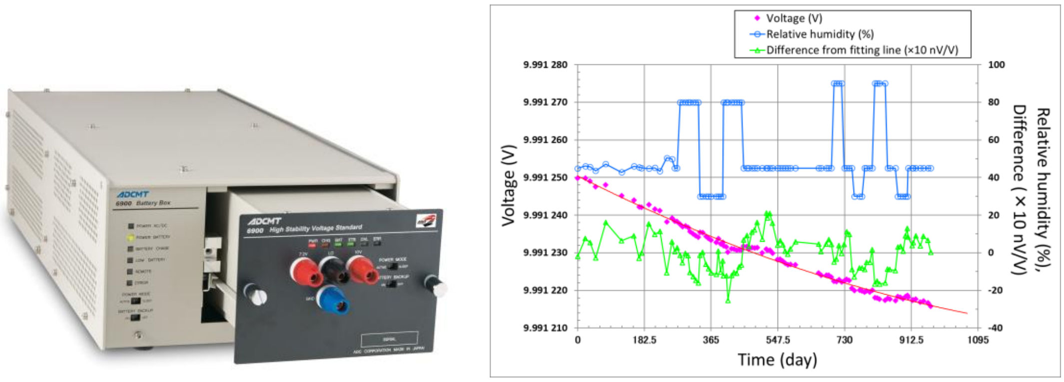

Fig.3.1 Prototype of a Zener votage standard and its relative-humidity dependence.

We measured the thermodynamic temperature of the melting point of gallium TGa using a Johnson noise thermometer (JNT) with an integrated quantum voltage noise source (IQVNS) as a reference. TGa was calculated using the fundamental constants recommended by the Committee on Data for Science and Technology (CODATA) for the revision of the International System of Units (SI). The measured TGa is consistent with the value defined in the International Temperature Scale of 1990.The power spectral density of output signal of IQVNS has been fixed so far. In order to use IQVNS as a reference for the measurement of thermodynamic temperature at various temperature fixed points, the power spectral density of the output signal of IQVNS should be variable. We improved part of the design of the device to be able to change the power spectral density of the output signal.

Development of compact and ultra-stable 1 Ω and 1 kΩ standard resistors has been finished, and resistors with 10 kΩ are in progress of evaluation and development. The best resistors display extremely small average drift rates and temperature coefficients, and other performances (Fig. 3.2), e.g.,

- 1 Ω: 4.2 nΩ/(Ω year), 4 nΩ/(Ω ˚C) at 23 ˚C,
- 10 Ω: 0.53 nΩ/(Ω year), 1 nΩ/(Ω ˚C) at 23 ˚C,
- 100 Ω: 50 nΩ/(Ω year), < 20 nΩ/(Ω ˚C) at 23 ˚C, deviation by transportation: < 10 nΩ/Ω, power and humidity coefficients are negligible,
- 1 kΩ: < 10 nΩ/(Ω year), 1.7 nΩ/(Ω ˚C) at 23 ◦C.

(note that the average drift rate and temperature coefficient of each resistance value does not come from the same resistor). It is demonstrated that this excellent performance is suitable for utilization in national metrology institutes and international comparisons.

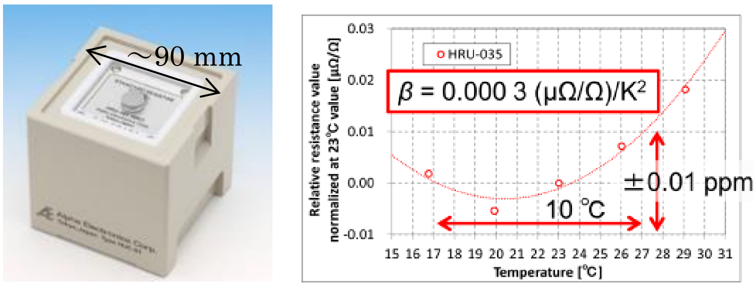

Fig. 3.2 Picture and temperature-resistance curve of developed 100 Ω standard resistor.

Some 1 MΩ quantum Hall array devices were fabricated and evaluated (Fig. 3.3). The devices have simple configuration and consist of 88 Hall bars. They have the nominal quantized resistance value of $10^6 \times (1 + 246.289 \times 10^{-6})$ Ω and its quantized value was evaluated using a cryogenic current comparator (CCC) bridge at NIST. The below graph shows the magnetic field dependence of the device. At the center of the plateau, the measurement was repeated some times and the measured value was scattered from −18 nΩ/Ω to +17 nΩ/Ω and the averaged value was +4 μΩ/Ω. The devices showed flat magnetic field dependence for more than 1 T.

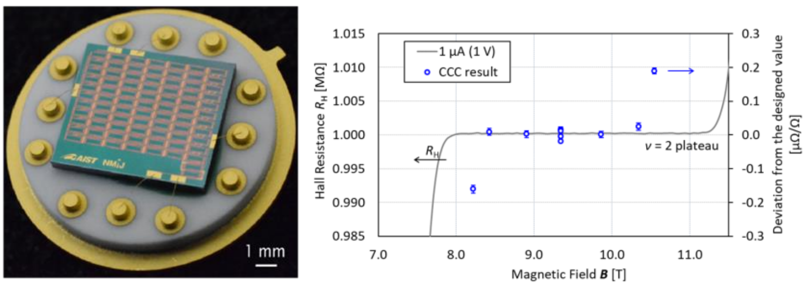

Fig. 3.3 Picture and the magnetic field dependence of the 1 MΩ array device.

To establish a relationship between the physical structure of electrical contact boundary and contact resistance, NMIJ developed a method for evaluating that using a physical simulated sample created via nanofabrication. Several samples with various distribution of "contact area" were made and their resistances were measured precisely. It was demonstrated experimentally that our result is in good agreement with an expression for constriction resistance.

Impedance measurement was introduced as a degradation diagnosis method for contacts of wire harness by a nondestructive test. It was found that the changes in reactance at a certain frequency behave characteristically and independently of the DC resistance changes during accelerated test. The degradation degree of contacts was estimated by the change in impedance.

Towards a realization of the current standard based on the single-electron pumping, we investigate the physics of low-temperature electron transport phenomena in various types of single-electron devices, i.e. superconductor-insulator-normal- insulator-superconductor (SINIS) turnstiles, gate-confined quantum dots, and graphene- or nanotube-based single-electron transistors.

On SINIS turnstiles, in our early studies, we had discovered the new phenomenon that is a reduction of the single-electron pumping error induced by a weak magnetic field applied to the device. The origin of this phenomenon is related to the suppression of inverse-proximity effect at the interface between superconducting leads and a normal metal island.

The inverse proximity effect causes the quasiparticle trap at the interface, namely it leads to the overheating of the junction. The magnetic field weaken the inverse proximity effect and helps to lease the quasiparticle. We justify this scenario from numerical analysis and controlling the tunnel resistance. Aiming at further reducing the pumping error, we extended the research to that based on another pumping mechanism. In one instance, we investigated a GaAs-based gate-defined quantum dot and demonstrated single-parameter pumping. In addition, we developed an air-bridge based parallel integration of this pump to demonstrate a synchronized parallel pumping that can generate a larger current otherwise unattained. In this study, we succeeded to operate the GaAs single electron device with sigma-delta modulated pulses for the arbitrary wave generation. This technique is thought to be useful for the calibration of current noise in the shot noise measurement. Also we start to measure the Si single electron pump device in collaboration with NTT group. At present we succeeded to operate single electron pumping at 1 GHz with 10^{-6} uncertainty. Now we try to operate this type of device in parallel to generate large (a few nano ampere) current.

These single-electron devices are planned to be integrated with the quantum metrology triangle experiment that combine the single-electron device with the quantum Hall resistance and Josephson voltage standards. Towards this futuristic experiment, we had introduced a dry dilution refrigerator; An ample open space offered by this refrigerator allows us to integrate the whole components required for the triangle experiment including a cryogenic current comparator into one system. Electric noise filters and high-frequency wiring are now designed and constructed to complete this setup. Also to operate Josephson voltage standard and quantum Hall array device inside the dilution refrigerator, we are installing additional cold stage and try to operate these quantum standards.

AC resistor calibration service has been kept in the range of 10 Ω up to 100 kΩ at 1 kHz and 10 kHz. Standard capacitor (dry-nitrogen or used silica dielectric) calibration service has been kept in the range of 10 pF up to 1000 pF at 1 kHz, 1.592 kHz.

NMIJ has started a development of precision measuring techniques for diagnosis of the energy storage devices such as lithium-ion batteries and super-capacitors by using an impedance spectroscopy method. We have a plan to establish a metrology for evaluating the storage power devices. Preliminary impedance measurements for lithium-ion battery cells in the range of 10 mHz – 10 kHz demonstrated that the impedance value for unused cells is clearly distinguished from that for used-up cells. Impedance spectra for the unused cells which are obtained under 100 mΩ indicate that the evaluations of the uncertainties should be required for detecting a faint sign or a symptom of degradations of storage devices. We have developed an electrochemical impedance measurement system and have evaluated the type-A uncertainty for the impedance spectra which was estimated to be less than 0.2 mΩ (Fig .3.4, Fig.3.5).

AIST established the Global Zero Emission Research Center (GZR) in 2020. GZR has a mission for an international joint research base for zero emission technologies. GZR started to research for innovative environmental and energy technologies, including in the fields of renewable energy, storage batteries, hydrogen, and so on. NMIJ joined in GZR and has started the research of the safety and reliability evaluation method for solid oxide electrochemical cells and lithium ion batteries by using precision impedance and charge-discharge measurements.

Fig. 3.4 Photograph of the electrochemical impedance measurement system developed using the Frequency Response Analyzer and the Potentio-Galvano Stat.

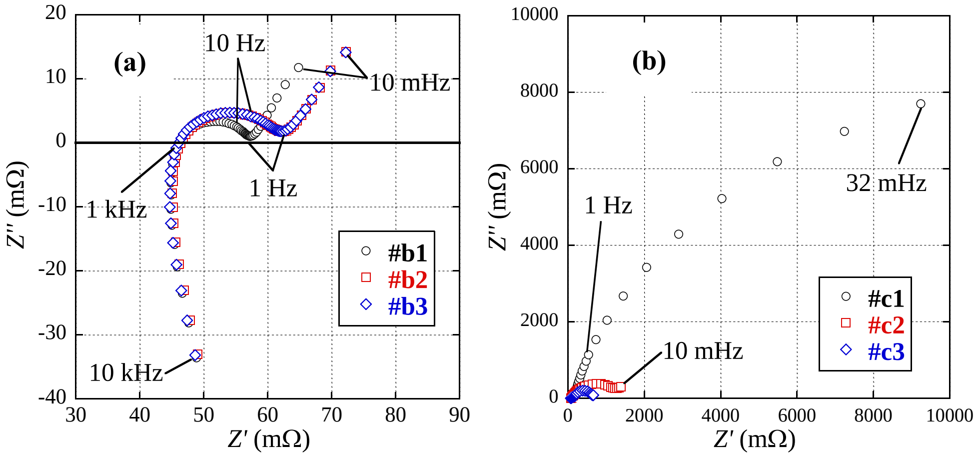

Fig. 3.5 Nyquist plot of the impedance spectra for the 18650-type lithium-ion batteries: (a) the unused samples and (b) used-up samples. Obvious change in impedance spectra was observed with the progression of the charge/discharge cycle.

NMIJ has provided ac-dc voltage difference transfer calibration of thermal converters in the voltage range from 10 mV to 1000 V and in the frequency range from 10 Hz to 1 MHz, and AC voltage calibration below 10 Hz. We have been participating in APMP Comparison for " APMP.EM-K12" of AC/DC current transfer difference, and “CCEM-K6a/K9” of AC/DC voltage transfer difference.

The thin film multi-junction thermal converters with a novel design have been developed at NMIJ/AIST in collaboration with NIKKOHM Co. Ltd. We have introduced a new thermopile pattern to improve the performance of our thin film MJTC [Amagi *et al.*, 2015a]. Using these thermal converters, novel thermal converter circuits arranged in an 2 by 2 matrix have been fabricated to improve the low-frequency AC-DC transfer differences [Amagai *et al.*, 2019]. Thin-film AC-DC resistor on an AlN substrate with negligible voltage dependence have been fabricated for measuring AC voltages up to 1000 V. Toward next-generation AC/DC current transfer standard, high-current multijunction thermal converters on Si substrates up to 1 A have been designed and fabricated through the collaborative project with NIST in Gaithersburg. The results were presented at NCSLI/CPEM2020 and a joint paper was submitted.

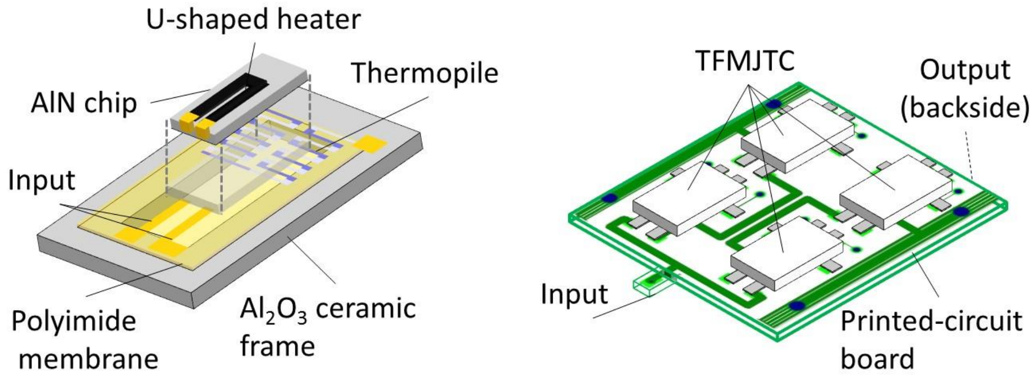

Fig. 6

Toward quantum AC voltage standards, a differential sampling measurement system using an AC-programmable Josephson voltage standard (AC-PJVS) system has been developed [Amagai *et al*., 2020]. To extend the voltage range of the system, we have combined a two-stage inductive voltage divider and an 10 V AC-programmable Josephson voltage standard chip.

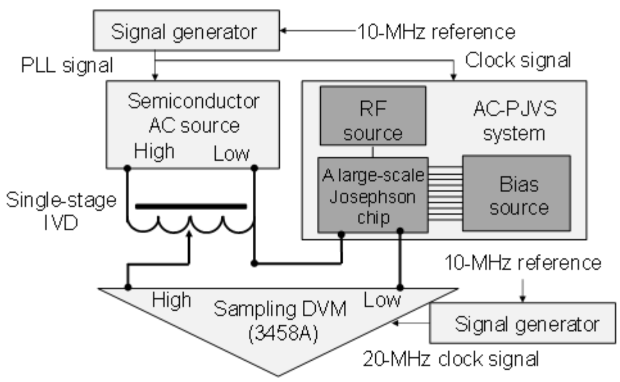

Fig. 7

Toward a waste-heat recovery with thermoelectric conversion, we have developed advanced metrology techniques and apparatus using a precise ac and dc electrical measurement technique. In particular, the Seebeck coefficient is an essential indicator of the conversion efficiency and the most widely measured property specific to these materials. So far, we have developed a method to precisely measure Thomson effect to determine the absolute Seebeck coefficient of platinum reference material [Amagai *et al*., 2015b] [Amagai *et al*., 2019b] [Amagai *et al*., 2020]. We have also precisely measured the absolute Seebeck coefficient of the fine Pt sample at low temperature below 100 K using a high-Tc superconductor as a reference [Amagai 2020].

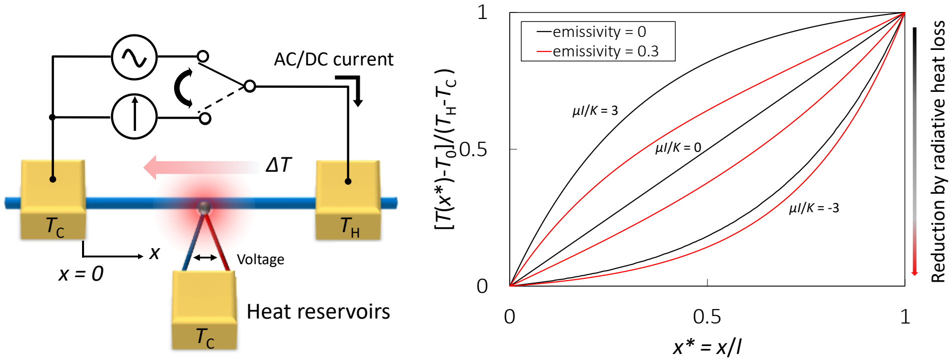

Fig. 8

[References]

Amagai Y, Fujiki H, Shimizume K, Kishino K and Hidaka S [2015a], "Improvements in the Low-Frequency Characteristic and Sensitivity of a Thin-Film Multijunction Thermal Converter in Vacuum," IEEE Trans. Instrum. Meas. **64**(6), 1570-1575, doi: 10.1109/TIM.2014.2385133.

Amagai Y, Fujiki H, Okawa K and Kaneko N [2019a], "Low-Frequency AC–DC Differences of a Series–Parallel Circuit of Thermal Converters," IEEE Trans. Instrum. Meas. **68**(6), 1907-1912, doi: 10.1109/TIM.2018.2882929.

Amagai Y, *et al*. [2020], Meas. Sci. Technol. **31**, 065010.

Amagai Y, Yamamoto A, Akoshima M, Fujiki H and Kaneko N [2015b], "AC/DC Transfer Technique for Measuring Thomson Coefficient: Toward Thermoelectric Metrology," IEEE Trans. Instrum. Meas. **64**(6), 1576-1581, doi: 10.1109/TIM.2014.2381752.

Amagai Y, Shimazaki T, Okawa K, Fujiki H, Kawae T, and Kaneko N-H, [2019b] AIP Advances **9**, 065312, https://doi.org/10.1063/1.5095485.

Amagai Y, Shimazaki T, Okawa K, Kawae T, Fujiki H, and Kaneko N-H, [2020a], Appl. Phys. Lett. **117**, 063903, https://doi.org/10.1063/5.0018593.

Amagai Y, Shimazaki T, Okawa K, Kawae T, Fujiki H, and Kaneko N-H, [2020b], Rev. Sci. Instrum. **91**, 014903, https://doi.org/10.1063/1.5122226.

A4. EM Field, Power Density and Antenna Measurement

At NMIJ, a calibration service for the free-space antenna factor on loop antenna is maintained in the frequency range of 20 Hz to 30 MHz. The expanded uncertainty of the magnetic antenna factor was improved to be from 0.4 dB to 0.7 dB in the frequency range from 9 kHz to 30 MHz in December 2019.

AC Magnetic field sensor calibration service is maintained in a range of 1 uT to 150 uT from 50 Hz to 100 kHz. The realizable field strength depends on frequency points.

NMIJ is also developing a novel EM-sonsor and an EM visualization method by using quantum phenomena of vapor cesium atoms.

[References]

[1] M. Ishii and M. Kinoshita, “A feasibility study of a real-time visualization method for electromagnetic fields,” Microw. Opt. Technol. Lett. **63**, 399-403 (2021).

[2] M. Ishii, “A study of frequency extension of AC magnetic field sensor using radio-optical multiple resonance in 133Cs,” EMC europe 2020, 2020.

[3] M. Ishii and M. Suzuki, “Impedance of Helmholtz Coils to Generate Standard AC Magnetic Fields in High Frequency,” 2020 Conference on Precision Electromagnetic Measurements (CPEM), 2020.

[4] M. Kinoshita and M. Ishii, “Visualization of radio-frequency waves via double resonance spectroscopy of cesium atoms,” Jpn. J. Appl. Phys. **58**(5), 052004-1-5 (2019).

[5] M. Ishii, “A feasibity study of AC magnetic field sensor in low-frequency using multi radiooptical resonance in 133Cs,” vol. 1, pp. 760, Proceedings of EMC Sapporo & APEMC 2019 (2019).

[6] M. Ishii, J. H. Kim, Y. Ji, and C. H. Cho, “Final report on APMP.RF-S21.F,” Metrologia **55**(1A), 01003 (2018).

Calibration of the dipole antenna factor above a ground plane from 30 MHz to 1 GHz with the specific conditions (with horizontal polarization and at 2.0 m from the ground plane surface) is available. Since EMC (electromagnetic compatibility) measurements are ordinarily carried out in free space above 1 GHz, the dipole antenna factor from 1 GHz to 2 GHz is calibrated in an anechoic chamber. The free space dipole factor is a traceability source of the E-field strength.

[References]

[1] T. Morioka, “Time-domain mixed-mode site attenuation measurement," IEEE Trans. on Electromagn. Compat. **62**(6), 2650-2660 (2020).

[2] T. Morioka, “Improvement of anechoic chamber performance by the time-domain analysis,”

in Proc. of EMC Sapporo and APEMC 2019, Sapporo, Japan, 2019.

The free space antenna factor calibration services for broadband antenna for Biconical antenna (30 MHz to 300 MHz), Log periodic dipole array antenna (300 MHz to 1000 MHz) and Super broadband antenna (30 MHz to 1000 MHz) are being performed using our original three antenna calibration method. The eight calibration services have been provided to the client in between 2018 and the present.

[References]

[1] S. Matsukawa and S. Kurokawa, "Antenna gain self-calibration for Double Ridged Guide Horn Antenna using bi-directional optical fiber link transceiver," ECTI-CON2019, pp. 1-4, Pattaya, Thailand, 10-13 July 2019.

[2] S. Matsukawa, S. Kurokawa and, M. Hirose, "Uncertainty Analysis of Far-Field Gain Measurement of DRGH Using the Single-Antenna Method and Amplitude Center Distance," IEEE Tran. Instrum. Meas. **68**(6), 1756-1754 (2019).

[3] S. Matsukawa, S. Kurokawa, M. Ameya and Y. She, "Influence of reflection area on calibration accuracy by single antenna method using broadband antenna," CPEM2018, pp. 1-2, Paris, France, 8-13 July, 2018.

An antenna factor calibration service for the broadband horn antenna (1 GHz to 18 GHz) is available using the time-domain single antenna extrapolation method in the semi-anechoic chamber.

An antenna gain calibration service for millimeter-wave standard gain horn antenna are being performed form 50 GHz to 75 GHz and 75 GHz to 110 GHz using a time-domain processing and extrapolation technique. Standard gain horn antenna calibration service for 220 GHz to 330 GHz has been started from March 2020. The expanded uncertainty of antenna gain was estimated to between 0.34 dB to 0.5 dB. The mm-wave antenna gain calibration by single antenna extrapolation method with moving flat-reflector is also studied.

[References]

[1] M. Ameya, S. Matsukawa and S. Kurokawa, "Antenna Gain Self-calibration Method with Moving Flat Reflector for Millimeter-wave Frequency Band," Proceedings of 2018 IEEE Conference on Antenna Measurements & Applications (CAMA), 2018

[2] M. Ameya and S. Kurokawa, "Development of Antenna Gain Calibration System in 300 GHz Frequency Band," Proceedings of 2019 URSI-Japan Radio Science Meeting, A2-4, 2019.

[3] M. Ameya, S. Matsukawa, and S. Kurokawa, "Uncertainty Estimation of Antenna Gain Self-

Calibration Method with Moving Flat Reflector for 5G Standard Gain Horn Antenna," Proceedings of IEEE CAMA 2019, pp.277-280, 2019.

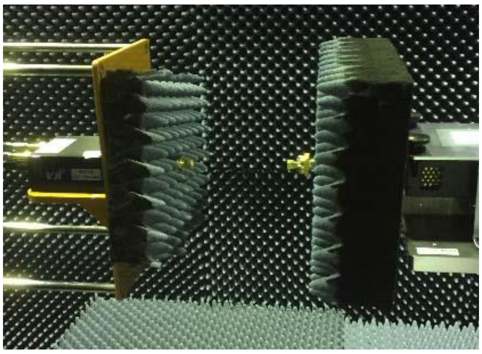

Fig. 12 Antenna gain calibration system to 330 GHz

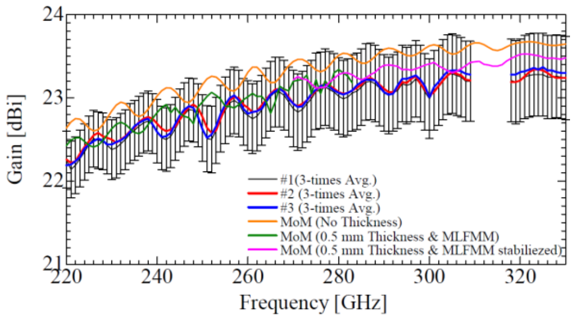

Fig. 13 Estimated antenna gain that compare for 220 with MoM results

Radar Cross Section (RCS) calibration service for cylindrical metal reflector and square metal plate in W-band has been started from March 2019. The expanded uncertainty of RCS for cylindrical metal reflector in W-band was estimated to between 1.1 to 1.6 dB. The expanded uncertainty of RCS for square metal plate reflector in W-band was estimated to between 1.4 dB to 2.1 dB.

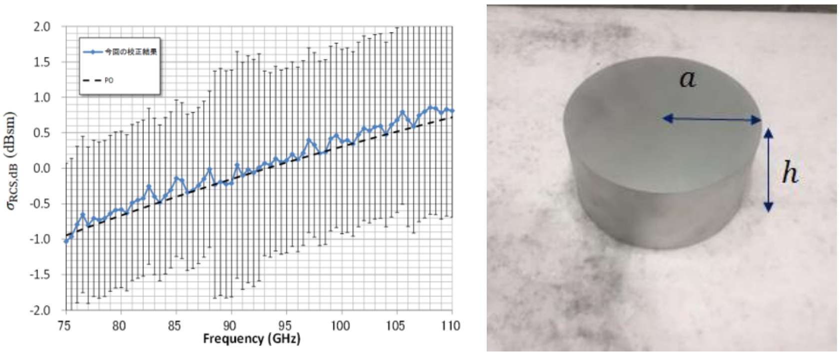

Fig. 14 RCS calibration results in W-band and an example of a cylindrical reflector

The E-field strength is one of the important quantities in the electromagnetic free field metrology and the field measurement is ordinarily carried out by using a calibrated E-field probe. In NMIJ/AIST, the correction factors of the E-field probe are calibrated against the field level of 10 V/m and 20 V/m generated in a G-TEM cell. Three appropriate methods to generate the standard E-field depending on the measurement frequency are employed in calibrating the response of the primary optical probe. A TEM cell is employed as a standard E-field generator at lower frequencies below 900 MHz, and the E-field level from 0.8 GHz to 2.2 GHz is calibrated by using the free space dipole antenna factor in the anechoic chamber. Antenna gain and the net power flowing into the transmitting antenna are the traceability sources for the standard field generation in the anechoic chamber from 2 GHz to 6 GHz. The calibrated optical E-field probe against these standard E-fields transfers the E-field level into the G-TEM cell, and then the ordinary field probe is calibrated up to 4 GHz.

[References]

[1] T. Morioka, “Reflectometer calibration for net power measurement and uncertainty,” in CPEM Dig., pp. 1-2, Denver CO, USA, Aug. 2020. (Virtual conference)

For the Radio Low in Japan, Calibration service of RF measurement instruments such as RF power meters, RF attenuators, and antennas has been performed by NICT.

Calibration service of RF power meters in the frequency range from 170-220 GHz and 220-330 GHz have been started in 2021 and 2018, respectively to realize spurious measurements in accordance with the ITU-R recommendation SM.32-10. It has been worked out by a collaboration between NICT and NMIJ [Tojima *et al*., 2020] [Kinoshita *et al*., 2018]. In addition, calibration service of RF power meter for 75 Ω system which is based on the Japan Calibration Service System (JCSS) has been started in 2019 to prepare with becoming widely use 4K/8K television system [Sakai *et al*., 2017]. Calibration service of RF power meters at 10 W (+40 dBm) in the frequency range from 10 MHz to 9 GHz is available, too.

Calibration service of loop antennas which is based on the JCSS has been performed using our original calibration method, which will be standardized by IEC/CISPR in 2022 [Fujii *et al*., 2017]. Calibration services of dipole antennas for 25-1,000 MHz, biconical antennas for 25-300 MHz, standard gain horn antennas for 1-40 GHz, and double-ridged guide antennas for 1-18 GHz are available.

[References]

Tojima Y, Kinoshita M, Iida H, and Fujii K [2020], “Calibrating Power Meters in the 140–220-GHz Frequency Range Using an Absolute-Power Reference Calorimeter,” IEEE Trans. on Intrum. Meas. **70**, 1002709.

Kinoshita M, Inoue T, Shimaoka K, and Fujii K [2018], “Precise power measurement with a single-mode waveguide calorimeter in the 220–330 GHz frequency range,” IEEE Trans. Instrum. Meas. **67**(6), 1451–1460.

Sakai K, Sugiyama T, Sebata K, Nishiyama I, and Fujii K [2017], “Power Meter Calibration 2 (1 mW, 75 Ω)," Journal of NICT **63**(1), 23-31.

Fujii K, Sakai K, Sugiyama T, Sebata K, and Nishiyama I [2017], "Calibration of Loop Antennas for EMI Measurements in the Frequency Range Below 30 MHz," Journal of NICT **63**(1), 71-81.

A5. Power Attenuation and Impedance Measurements

The Applied Electronics Standards Group, the Radio-Frequency Group and the Electromagnetic Measurement Group in the elctrical standards area of NMIJ covers the A5 fields.

The phase difference measurement system based on the three-voltmeter method (3VM) and a differential thermal voltage converter (TVC) has been checked for frequency range from 1 kHz to 1 MHz (Fig. 5.1). It has been found that the differential thermal voltage converter has a large amount of differential voltage measurement error over the frequency of 100 kHz. A measurement method of a differential TVC AC/DC difference has been developed to make the large error reduced for the frequency range.

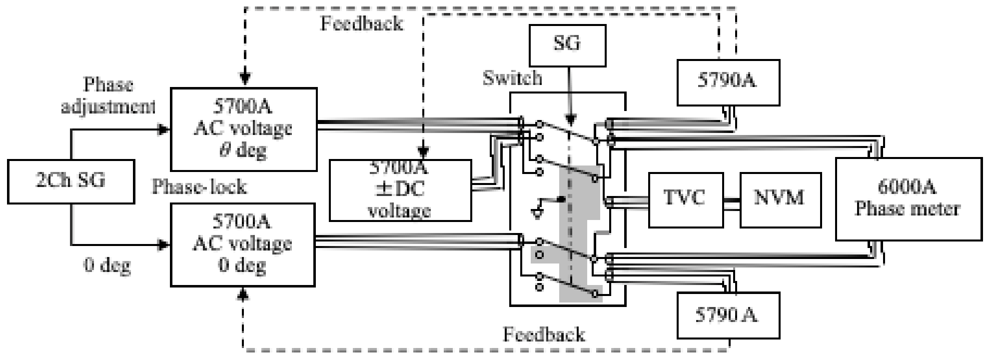

The 3VM-based phase difference measurement system.

Fig. 5.1

JEMIC has provided the primary active/reactive power/energy standards for the power frequencies in the voltage range from 50 V to 120 V and in the current range from 2.5 A to 50 A. The standard individually measures voltage U and current I with two precise voltmeters and a shunt resistor, and phase θ with a precise digital phase meter. After these measurements, the active and reactive powers are calculated by $UI\cos\theta$ and $UI\sin\theta$, respectively. The representative expanded uncertainties under conditions of 100 V and 5 A are 22 μW/VA (power factor 1) and 10 μW/VA (power factor 0). In 2019, we calibrated approximately 10 power meters and 70 energy meters.

NMIJ developed a WR-5 waveguide-based calorimeter for the frequency range of 140-220 GHz in collaboration with NICT. Direct comparison calibration was demonstrated for commercially available power meters using the calorimeter as a reference standard. We have begun to provide reference values for the WR-5 band to domestic organizations.

NMIJ has established national standard for RF and microwave attenuation in the frequency range of 100 kHz to 110 GHz, and provides its calibration services mainly with the Japan Calibration Service System (JCSS) scheme. All measurement and calibration systems work based on the intermediate frequency (IF) substitution method using the highly accurate null detection and employing an inductive voltage divider (IVD) as the reference standard. Improvements including measurement system in the 1 kHz to 100 kHz frequency range (Fig. 5.2) are conducting to meet industry requirements regarding electromagnetic compatibility (EMC).

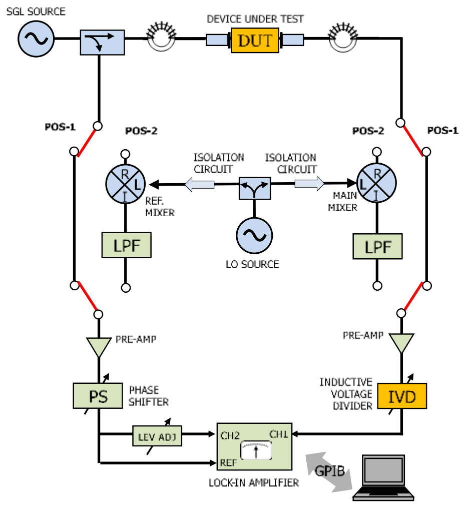

Fig. 5.2

NMIJ established national standard for RF phase shift in the frequency range of 10 MHz to 1 GHz. The expanded uncertainties are 0.029° for DUT with losses up to 20 dB, 0.031° for 40 dB, and 0.056° for 60 dB loss. The frequency range is currently being expanded to 18 GHz.

NMIJ took an initiative to organize a CIPM Key Comparison of attenuation at 18 GHz, 26.5 GHz and 40 GHz using a step attenuator. Measurements of both the first and second round loop were completed on February 2018. It can be said successful, although there were some delays in the delivery of the traveling standards between the participants. Preparation of the Draft A report is started.

NMIJ researched the precision on-wafer measurement techniques over 100 GHz and developed a full-automatic RF probing system establishing high reproducibility of measurements. Balanced type circular disk resonator method has been developped and commarcialized, in addition, the method will be published as an IEC standardization. The method cannot only measure dielectric permittivity but also conductivity at millimeter wave frequency (Fig. 5.3). Furthermore, electromagnetic sensing techniques is also researching for the agriculture products, food and infrastructure, etc.. In addition, scanning microwave microscopy (SMM) technique are researching and NMIJ originally developed matching circuit to establish high sensitivity and low signal-to-noise ratio. Recently, NMIJ demonstrated percoemance comparison for three SMM system.

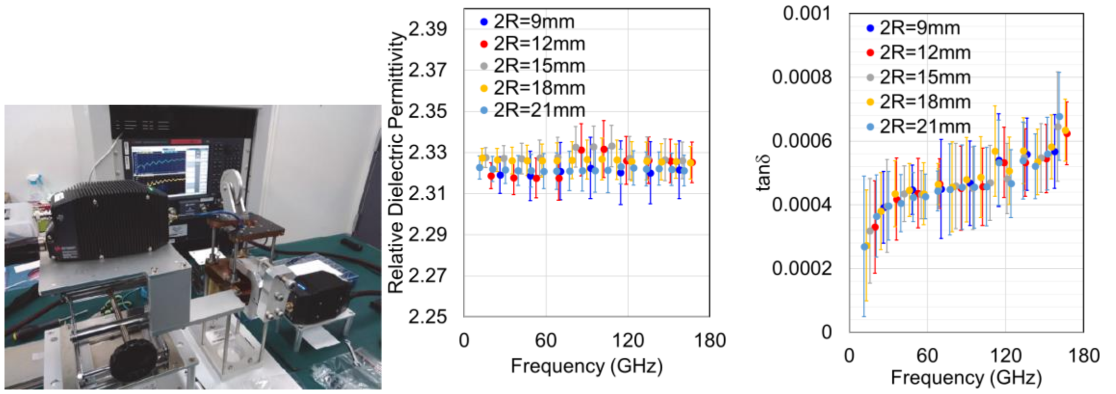

Fig. 5.3

NMIJ as a pilot laboratory is managing the CCEM key comparison (CCEM.RF-K5c.CL: S-parameter for PC3.5 in the range from 50 MHz to 33 GHz), the APMP supplemental comparison (APMP.EM.RF-S5.CL: Dimensionally-derived characteristic impedance for PC7, PC2.4 and PC1.85) and the pilot study for material characterization.

NMIJ has developed a highly sensitive terahertz calorimeter using a broadband absorber (Fig. 5.4). A magnetically loaded epoxy having a pyramidal surface was used as the absorber. The calorimeter enabled the measurement of absolute power from 110 GHz to several THz. The measurement uncertainties were 6.2% for 13 μW at 300 GHz and 5.6% for 1.5 μW at 1 THz (k=2). We also have demonstrated a THz power measurement of tens of nanowatts at room temperature using the calorimeter with vacuum insulation panels utilized for thermal insulation. The absolute power of 26.7 nW was measured at 1 THz with the expanded uncertainty of 4.2% (k=2).

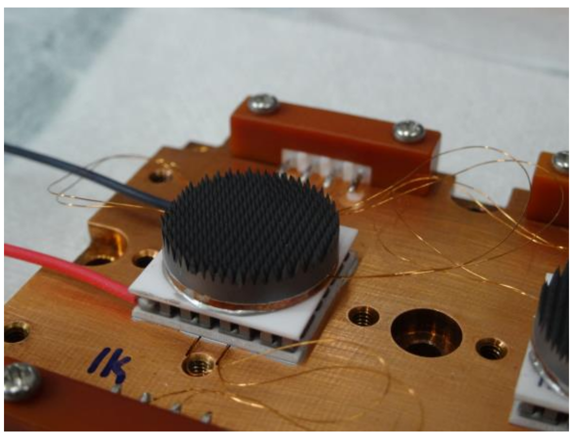

Fig. 5.4

NMIJ developed a method for measuring terahertz (THz) attenuation for free-space beams (Fig. 5.5). It employs a photo-acoustic detector to compare THz attenuation to audio-frequency (AF) attenuation. The AF attenuation is directly calibrated by an inductive voltage divider as a reference standard. Using a metalized-film attenuator, we have demonstrated attenuation measurements up to 20 dB for 0.11 THz collimated beams.

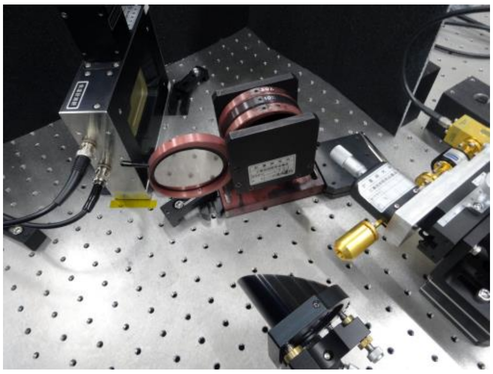

Fig. 5.5

NMIJ is researching and develops material characterization, i.e. dielectric permittivity measurements, at the millimeterwave frequency. NMIJ developed the Balanced-type circular-disk resonator (BCDR) and analytical sofware for dielectroic permittivity of low loss materials. Measurement can be performed in broad band frequency and up to 120 GHz (Fig. 5.6). The method is now being standardized in the IEC standard, then the system has been provided by the measurement instrument company.

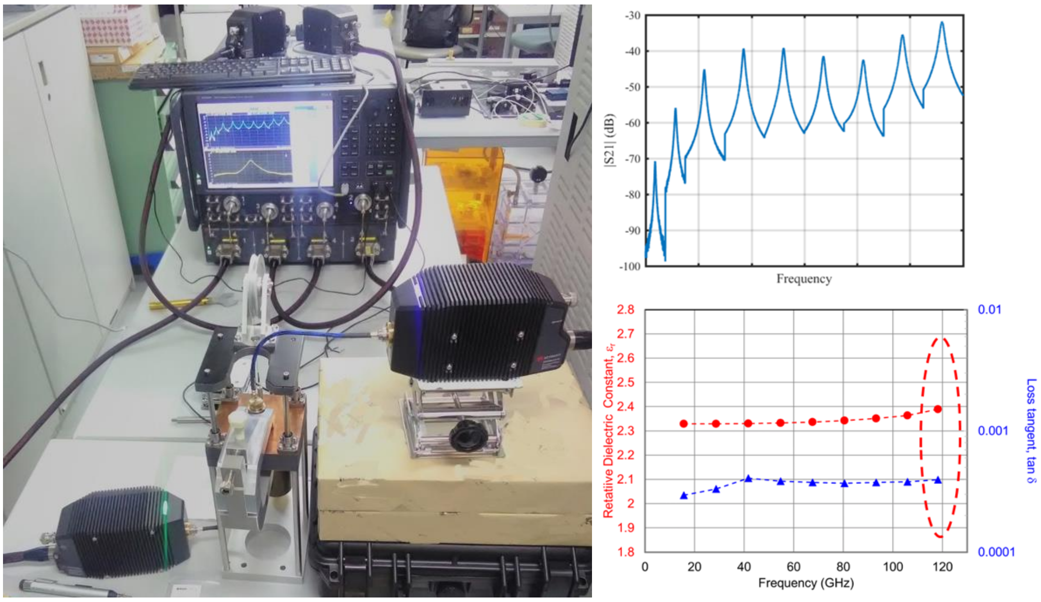

Fig. 5.6